Technical Note: Improved partial wavelet coherency for understanding scale-specific and localized bivariate relationships in geosciences

Wei Hu[1] and Bing Si[2]

[1]*The New Zealand Institute for Plant and Food Research Limited, Private Bag 4704, Christchurch 8140, New Zealand*

[2]*University of Saskatchewan, Department of Soil Science, Saskatoon, SK S7N 5A8, Canada*

Correspondence to: Wei Hu (wei.hu@plantandfood.co.nz)

Abstract

Bivariate wavelet coherency is a measure of correlation between two spatial (or time) series in the location-scale (or time-frequency) domain. It is particularly suited to geoscience where relationships between multiple variables commonly differ with locations or/and scales because of various processes involved. However, it is well-known that bivariate relationships can be misleading when both variables are dependent on other variables. Partial wavelet coherency (PWC) has been proposed to detect the scale-specific and localized bivariate relationships by excluding the effects of other variables, but is limited to one excluding variable and presents no phase information. We aim to develop a new PWC method that can deal with multiple excluding variables and presents phase information. Both stationary and non-stationary artificial datasets with the response variable being the sum of five cosine waves at 256 locations are used to test the methods.

The new method was also applied to a free water evaporation dataset. Our results verified the advantages of the new method in capturing phase information and dealing with multiple excluding variables. Compared with the previous PWC calculation, the new method produces more accurate results where there is one excluding variable. This is because bivariate real coherence rather than the bivariate complex coherence was mistakenly used in the previous PWC calculation, which underestimates the PWC. We suggest the PWC method to be used in combination with previous wavelet methods to untangle the scale-specific and localized multivariate relationships in geosciences. The PWC calculations were coded with Matlab and are freely accessible (https://figshare.com/s/bc97956f43fe5734c784).

1. Introduction

Geoscience data, such as spatial distribution of soil moisture in undulating terrains and time series of climatic variables, usually consist of a variety of transient processes with different scales or frequencies that may be localized in space or time (Torrence and Compo, 1998; Si, 2008; Graf et al., 2014). For example, time series of air temperature usually fluctuates periodically at different scales (e.g., daily and yearly), but abrupt changes in air temperature (e.g., extremely high or low) may occur at certain time points as a result of extreme weather and climate events (e.g., heat and rain). Wavelet methods are widely used to detect scale-specific and localized features of geoscience data irrespective of whether they are stationary or non-stationary.

Wavelet analyses are based on wavelet transform using mother wavelet function which expands spatial (or time) series into location-scale (or time-frequency) space for identification of localized intermittent scales (or frequencies). For convenience, we will mainly refer to location and scale irrespective of spatial or time series unless otherwise mentioned. Among these wavelet methods, bivariate wavelet coherency (BWC) is widely accepted as a tool for detecting scale-specific and localized bivariate relationships in a range of areas in geoscience (Lakshmi et al., 2004; Si and Zeleke, 2005; Das and Mohanty, 2008; Polansky et al., 2010; Biswas and Si, 2011). The BWC partitions correlation between two variables into different locations and scales, which are different from the overall relationships at the sampling scale as shown by the traditional correlation coefficient. For example, BWC analysis indicated that soil water content of a hummocky landscape in the Canadian Prairies was negatively correlated to soil organic carbon content at a slope scale (50 m), but they were positively correlated at a watershed scale (120 m) in summer because of the different processes involved at different scales (Hu et al., 2017). Because the positive correlation may cancel out with the negative at different scales and/or locations, the traditional correlation coefficient between soil water content and soil organic carbon content does not differ significantly from zero, which is misleading.

Recently, Hu and Si (2016) have extended the BWC to multiple wavelet coherence (MWC) that can be used to untangle multivariate ($\geq$3 variables) relationships in multiple location-scale domains. This method has been successfully used in hydrology (Hu et al., 2017; Nalley et al., 2019; Su et al., 2019; Gu et al., 2020; Mares et al., 2020) and other areas such as soil science (Centeno et al., 2020), environmental science (Zhao et al., 2018), meteorology (Song et al., 2020), and economics (Sen et al., 2019). The MWC application has shown that an increased number of predictor variables does not necessarily explain more variations in the response variable, partly because predictor variables are usually cross-correlated (Hu and Si, 2016). For the same reason, bivariate relationships can be misleading if the predictor variable is correlated with other variables that control the response variable. Partial correlation analysis is one such method to avoid the misleading relationships resulting from the interdependence between other variables and both predictor and response variables (Kenney and Keeping, 1939), but the extension of partial correlation to the multiple location-scale domain is limited. In order to better understand the bivariate relationships at multiple scales and locations, the BWC needs to be extended to partial wavelet coherency (PWC) by eliminating the effects of other variables.

The BWC was extended to PWC by Mihanović et al. (2009). Their method has been widely used in the areas of marine science (Ng and Chan, 2012a, b), meteorology (Tan et al., 2016; Rathinasamy et al., 2017), and economics (Aloui et al., 2018; Altarturi et al., 2018a; Wu et al., 2020), as well as in the study of greenhouse gas emissions (Jia et al., 2018; Li et al., 2018; Mutascu and Sokic, 2020), among others. For example, PWC analysis indicated that Southern Oscillation Index and Pacific Decadal Oscillation did not affect precipitation across India, while this was misinterpreted by the BWC analysis because of their interdependence on Niño 3.4 that affects precipitation (Rathinasamy et al., 2017). However, Mihanović et al. (2009) considered one excluding variable (i.e., variable that influences the response variable is excluded) only and did not include the phase angle difference between response and predictor variables. The coherence between response and predictor variables can still be misleading if more than one variable is interdependent with the predictor variable. This is especially true if these variables are correlated with the predictor variable at different locations and/or scales. In addition, without phase information, it is hard to tell if the correlation at a location and scale is positive or negative.

As an extension of previous studies (Mihanović et al., 2009; Hu and Si, 2016), this paper aims to develop a PWC method that considers more than one excluding variable and presents phase information. This method reveals the magnitude and type of bivariate relationships after removing the effects from all potentially interdependent variables. The new method is an extension from the multi-variate partial coherency in the frequency (scale) domain (Koopmans, 1995). The proposed method is first tested with artificial datasets following Yan and Gao (2007) and Hu and Si (2016) to demonstrate its capability of capturing the known relationships of the artificial data. Then it is applied to a real dataset, i.e., time series of free water evaporation at the Changwu site in China (Hu and Si, 2016). Finally, the advantages and weaknesses of the new method are discussed by comparing it with the previous PWC method.

2. Theory

Wavelet analysis is based on the calculations of wavelet coefficients using wavelet transform at different locations and scales for each variable involved. Two types of wavelet transform exist including continuous wavelet transform and discrete wavelet transform. While the discrete wavelet transform is mainly used for data compression and noise reduction, the continuous wavelet transform is widely used for extracting scale-specific and localized features, as is the case of this study (Grinsted et al., 2004). For the continuous wavelet transform, the Morlet wavelet is used as a mother wavelet function to transform a spatial (or time) series into location-scale (or time-frequency) domain, which allows us to identify both location-specific amplitude and phase information of wavelet coefficients at different scales (Torrence and Compo, 1998). From wavelet coefficients, auto- and cross-wavelet power spectra for two variables can be calculated as the product of wavelet coefficient and the complex conjugate of itself (auto-wavelet power spectra) or another variable (cross-wavelet power spectra). The BWC is calculated as the ratio of smoothed cross-wavelet power spectra of two variables to the product of their auto-wavelet power spectra (Grinsted et al., 2004). Hu and Si (2016) extended wavelet coherence from two to multiple (≥3) variables and developed MWC. Detailed information on the calculations of wavelet coefficients, auto- and cross-wavelet power spectra, BWC, and MWC based on the continuous wavelet transform can be found elsewhere (Torrence and Compo, 1998; Grinsted et al., 2004; Si and Farrell, 2004; Si, 2008; Hu and Si, 2016; Hu et al., 2017). Here, we will only introduce the theory and calculation that is very relevant to the PWC.

Similar to BWC and MWC, PWC is calculated from auto- and cross-wavelet power spectra, for the response variable y, predictor variable x, and excluding variables Z ($Z = \{Z_1, Z_2, \cdots, Z_q\}$). Koopmans (1995) developed the multivariate complex PWC in the frequency (scale) domain. Here, we extend the Koopmans (1995) method from the frequency (scale) domain to the time-frequency (location-scale) domain. Therefore, the complex PWC between y and x after excluding variables Z at scale s and location τ, $\gamma_{y,x\cdot \mathrm{Z}}(s,\tau)$, can be written as

$$\gamma_{y,x\cdot \mathrm{Z}}(s,\tau) = \frac{\left(1 - R^2_{y,x,Z}(s,\tau)\right)\, \gamma_{y,x}(s,\tau)}{\sqrt{\left(1 - R^2_{y,Z}(s,\tau)\right)\left(1 - R^2_{x,Z}(s,\tau)\right)}} \qquad (1)$$

where $R^2_{yx,Z}(s,\tau)$, $R^2_{y,Z}(s,\tau)$, and $R^2_{x,Z}(s,\tau)$ can be calculated by following Hu and Si (2016) as

$$R^2_{y,x,Z}(s,\tau) = \frac{\overset{\leftrightarrow}{W}^{y,Z}(s,\tau)\, \overset{\leftrightarrow}{W}^{Z,Z}(s,\tau)^{-1}\, \overline{\overset{\leftrightarrow}{W}^{x,Z}(s,\tau)}}{\overset{\leftrightarrow}{W}^{y,x}(s,\tau)} \qquad (2)$$

$$R^2_{y,Z}(s,\tau) = \frac{\overset{\leftrightarrow}{W}^{y,Z}(s,\tau)\, \overset{\leftrightarrow}{W}^{Z,Z}(s,\tau)^{-1}\, \overline{\overset{\leftrightarrow}{W}^{y,Z}(s,\tau)}}{\overset{\leftrightarrow}{W}^{y,y}(s,\tau)} \qquad (3)$$

$$R^2_{x,Z}(s,\tau) = \frac{\overset{\leftrightarrow}{W}^{x,Z}(s,\tau)\, \overset{\leftrightarrow}{W}^{Z,Z}(s,\tau)^{-1}\, \overline{\overset{\leftrightarrow}{W}^{x,Z}(s,\tau)}}{\overset{\leftrightarrow}{W}^{x,x}(s,\tau)} \qquad (4)$$

Eq. (1) can be also derived analogously from the complex partial spectrum for the frequency domain and the definition of complex coherence between two variables in the time-frequency domain (see the Supplement (Sect. S1) for the derivation process). Note that $R^2_{y,x\cdot Z}(s,\tau)$ is a matrix with complex values while $R^2_{y,Z}(s,\tau)$ and $R^2_{x,Z}(s,\tau)$ are matrices with real numbers. $\gamma_{y,x}(s,\tau)$ is the complex wavelet coherence between y and x, which can be written as

$$\gamma_{y,x}(s,\tau) = \frac{\overset{\leftrightarrow}{W}^{y,x}(s,\tau)}{\left(\overset{\leftrightarrow}{W}^{y,y}(s,\tau)\overset{\leftrightarrow}{W}^{x,x}(s,\tau)\right)^{1/2}} \qquad (5)$$

where $\underset{(\cdot)}{\leftrightarrow}$ is the smoothing operator, $\overline{(\cdot)}$ is the complex conjugate operator, $(\cdot)^{-1}$ indicates the inverse of the matrix, and

$$\overleftrightarrow{W}^{y,Z}(s,\tau) = \left[\overleftrightarrow{W}^{y,Z_1}(s,\tau)\,\overleftrightarrow{W}^{y,Z_2}(s,\tau)\cdots\overleftrightarrow{W}^{y,Z_q}(s,\tau)\right] \tag{6}$$

$$\overleftrightarrow{W}^{x,Z}(s,\tau) = \left[\overleftrightarrow{W}^{x,Z_1}(s,\tau)\,\overleftrightarrow{W}^{x,Z_2}(s,\tau)\cdots\overleftrightarrow{W}^{x,Z_q}(s,\tau)\right] \tag{7}$$

$$\overleftrightarrow{W}^{Z,Z}(s,\tau) = \begin{bmatrix} \overleftrightarrow{W}^{Z_1,Z_1}(s,\tau) & \cdots & \overleftrightarrow{W}^{Z_1,Z_q}(s,\tau) \\ \vdots & \ddots & \vdots \\ \overleftrightarrow{W}^{Z_q,Z_1}(s,\tau) & \cdots & \overleftrightarrow{W}^{Z_q,Z_q}(s,\tau) \end{bmatrix} \tag{8}$$

where $\overleftrightarrow{W}^{A,B}(s,\tau)$ is the smoothed auto-wavelet power spectra (when *A*=*B*) or cross-wavelet power spectra (when *A*≠*B*) at scale *s* and location τ, respectively.

The squared PWC (hereinafter referred to as PWC) at scale *s* and location τ, $\rho^2_{y,x\cdot Z}$, can be written as

$$\rho^2_{y,x\cdot Z} = \frac{\left|1-R^2_{y,x,Z}(s,\tau)\right|^2 R^2_{y,x}(s,\tau)}{\left(1-R^2_{y,Z}(s,\tau)\right)\left(1-R^2_{x,Z}(s,\tau)\right)} \tag{9}$$

where $R^2_{y,x}(s,\tau)$ is squared BWC between y and x, which can be expressed as

$$R^2_{y,x}(s,\tau) = \frac{\overleftrightarrow{W}^{y,x}(s,\tau)\overline{\overleftrightarrow{W}^{y,x}(s,\tau)}}{\overleftrightarrow{W}^{y,y}(s,\tau)\overleftrightarrow{W}^{x,x}(s,\tau)} \tag{10}$$

The phase angle (i.e., angle between two complex numbers) between y and x after excluding effect of Z is

$$\vartheta_{y,x\cdot Z}(s,\tau) = \varphi_{y,x\cdot Z}(s,\tau) + \vartheta_{y,x}(s,\tau) \tag{11}$$

where

$$\varphi_{y,x\cdot Z}(s,\tau) = \arg\left(1 - R^2_{y,x,Z}(s,\tau)\right) \tag{12}$$

and $\vartheta_{y,x}(s,\tau)$ is the wavelet phase between y and x, which can be expressed as

$$\vartheta_{y,x}(s,\tau) = \tan^{-1}\left(\mathrm{Im}\left(W^{y,x}(s,\tau)\right)/\mathrm{Re}\left(W^{y,x}(s,\tau)\right)\right) \quad (13)$$

where arg denotes the argument of the complex number, $W^{y,x}(s,\tau)$ is the cross-wavelet power spectrum between y and x at scale s and location τ; Im and Re denote the imaginary and real part of $W^{y,x}(s,\tau)$, respectively.

When only one variable (e.g., $Z1$) is excluded, Eq.(9) can be written as (see the Supplement (Sect. S2) for the derivation process)

$$\rho^2_{y,x\cdot Z1} = \frac{\left|\gamma_{y,x}(s,\tau) - \gamma_{y,Z1}(s,\tau)\overline{\gamma_{x,Z1}(s,\tau)}\right|^2}{\left(1-R^2_{y,Z1}(s,\tau)\right)\left(1-R^2_{x,Z1}(s,\tau)\right)} \quad (14)$$

The widely used Monte Carlo method (Torrence and Compo, 1998; Grinsted et al., 2004; Si and Farrell, 2004) is used to calculate PWC at the 95% confidence level. In brief, the PWC calculation is repeated for a sufficient number of times using data generated by Monte Carlo simulations based on the first-order autocorrelation coefficient (r1). The first-order autoregressive model (AR(1)) is chosen because it can be used to simulate most geoscience data very well (Wendroth et al., 1992; Grinsted et al., 2004; Si and Farrell, 2004). Different combinations of r1 values (i.e., 0.0, 0.5, and 0.9) were used to generate 10 to 10 000 AR(1) series with three, four and five variables. Our results indicate that the noise combination has little impact on the PWC values at the 95% confidence level as also found by Grinsted et al. (2004) for the BWC case (data not shown). The relative difference of PWC at the 95% confidence level compared with that calculated from the 10 000 AR(1) series decreases with the increase in number of AR(1) series. When the number of AR(1) is above 300, a very low maximum relative difference (e.g., <2%) is observed (Fig. S1 of Sect. S3 in the

Supplement). Therefore, a repeating number of 300 seems to be sufficient for a significance test. However, if calculation time is not a barrier, a higher repeating number, such as ≥1000, is recommended. The 95th percentile of PWCs of all simulations at each scale represents the PWC at the 95% confidence level. The average PWC, percent area of significant coherence (PASC) relative to the whole wavelet location–scale domain, and average value of significant PWC (PWC_{sig}) are also calculated for different location–scale domains.

In the case of one excluding variable ($Z = \{Z_1\}$), Mihanović et al. (2009) suggested that the PWC can be calculated by an equation analogous to the traditional partial correlation squared (Kenney and Keeping, 1939) without giving the detailed derivation process. Their equation is the same as Eq. (14). Unfortunately, Ng and Chan (2012a) might have misinterpreted the equation of Mihanović et al. (2009) and developed Matlab code for calculating PWC using the equation expressed as

$$\rho^2_{y,x\cdot Z1} = \frac{\left|R_{y,x}(s,\tau) - R_{y,Z1}(s,\tau)\, R_{x,Z1}(s,\tau)\right|^2}{\left(1 - R^2_{y,Z1}(s,\tau)\right)\left(1 - R^2_{x,Z1}(s,\tau)\right)} \tag{15}$$

where $R_{y,x}(s,\tau)$, $R_{y,Z1}(s,\tau)$, and $R_{x,Z1}(s,\tau)$ are the square root of $R^2_{y,x}(s,\tau)$, $R^2_{y,Z1}(s,\tau)$, $R^2_{x,Z1}(s,\tau)$, respectively. $R^2_{y,Z1}(s,\tau)$ and $R^2_{x,Z1}(s,\tau)$ can be calculated from Eq. (10) by replacing y and x with their corresponding variables. Eq. (15) has been widely used to calculate PWC in the case of one excluding variable (Ng and Chan, 2012b; Rathinasamy et al., 2017; Aloui et al., 2018; Altarturi et al., 2018b; Jia et al., 2018; Li et al., 2018; Mutascu and Sokic, 2020; Wu et al., 2020). Note that complex coherence and real coherence are involved in the numerators of Eqs. (14) and (15), respectively, while the denominators are exactly the same. Further comparison indicates that Eq. (15) underestimates PWC value relative to Eq. (14) unless $\gamma_{y,x}(s,\tau)$ and $\gamma_{y,Z1}(s,\tau)\,\overline{\gamma_{x,Z1}(s,\tau)}$ in Eq. (14) are collinear (i.e., their arguments are identical) under which the two equations produce the same PWC values. Differences between Eqs. (14) and (15) will be discussed further using both artificial data and a real dataset. For comparison purposes, we refer to Eqs. (14) and (15) as the new method and the classical method, respectively.

3. Method test using artificial data

3.1 Artificial data and analysis

The PWC is first tested using the cosine-like artificial dataset produced following Yan and Gao (2007). The cosine-like artificial datasets are suitable for testing the new method because they mimic many spatial or temporal series in geoscience such as climatic variables, hydrologic fluxes, seismic signals, El Niño-Southern Oscillation, land surface topography, ocean waves, and soil moisture. The procedures to test the PWC is largely based on Hu and Si (2016), where the same dataset has been used to test the MWC method (refer to Hu and Si (2016) for a detailed description of the artificial dataset). The response variable (y and z for the stationary and non-stationary case, respectively) is the sum of five cosine waves (y_1 to y_5 and z_1 to z_5 for the stationary and non-stationary case, respectively) at 256 locations (Hu and Si, 2016). For y_1, y_2, y_3, y_4, and y_5, they have consistent dimensionless scales of 4, 8, 16, 32, and 64, respectively, across the series. For z_1, z_2, z_3, z_4, and z_5, the dimensionless scales gradually change with location, with the maximum dimensionless scales of 4, 8, 16, 32, and 64, respectively. The variance of the response variable y and z is 2.5. All other variables (y_1 to y_5 or z_1 to z_5) are orthogonal to each other with equal variance of 0.5. The predictor and excluding variables (Fig. S1 of Sect. S4 in the Supplement) are selected from the five cosine waves (e.g., y_1 to y_5 or z_1 to z_5) or their derivatives. The exact variables and procedures to test the new PWC method are explained below.

The PWC between response variable y (or z) and predictor variable, i.e., y_2 (or z_2), is first calculated after excluding the effect of one variable. Four types of excluding variable are involved (Fig. S2 of Sect. S4 in the Supplement): (a) original series of y_2 (or z_2) or y_4 (or z_4); (b) second half of the original series of y_2 (or z_2) are replaced by 0 to simulate abrupt changes (i.e., transient and localized feature) of the spatial series. They are referred to as y_2h_0 (*or* z_2h_0); (c) white noises with zero-mean and standard deviations of 0.3 (weak noise), 1 (moderate noise), and 4 (high noise) are added to y_2 (or z_2) as suggested by Hu and Si (2016) to simulate non-perfect cyclic patterns of the excluding variables. They are referred to as y_2wn (*or* z_2wn), y_2mn (*or* z_2mn), and y_2sn (*or* z_2sn), respectively; and (d) a combination of type b and type c. They are referred to as y_2wnh_0 (*or* z_2wnh_0), y_2mnh_0 (*or* z_2mnh_0), and y_2snh_0 (*or* z_2snh_0), respectively.

The PWC between response variable y (or z) and predictor variable, i.e., y_2y_4 (sum of y_2 and y_4) for the stationary case or z_2z_4 (sum of z_2 and z_4) for the non-stationary case, is calculated with two excluding variables, which is a combination of y_4 (or z_4) and y_2 (or z_2) or its noised series (y_2wn *or* z_2wn, y_2mn *or* z_2mn, and y_2sn *or* z_2sn). Note that PWC between y (or z) and other predictor variables (e.g., y_4 or z_4) after excluding y_2 or z_2 and their equivalent derivative variables (i.e., noised variables or variables with 0) are also calculated.

The related results are not shown because they are analogous to those in case of predictor variable of y_2 (or z_2).

The merit of the artificial data is that we know the exact scale-specific and localized bivariate relationships after the effect of excluding variables is removed. Theoretically, we expect (a) PWC is 1 at scales corresponding to scale difference of excluding variables from predictor variable, and 0 at other scales. For example, PWC between y and y_2y_4 after excluding the effect of y_4 is expected to be 1 at the scale of 8, which is the difference of y_4 (32) from y_2y_4 (8 and 32), and 0 at other scales (e.g., 32); (b) PWC remains 1 at the second half of series where spatial series is replaced by 0, and 0 at the first half of the original series. For example, PWC between y and y_2 after excluding the effect of y_2h_0 is expected to be 0 and 1 at the first and second half of series, respectively, at the scale of 8; and (c) PWC increases as more noises are included in the excluding variables. For example, PWC between y and y_2 after excluding the effect of noised series of y_2 is expected to increase with increasing noises in an order of $y_2sn>y_2mn>y_2wn$ at the scale of 8.

3.2 PWC with artificial data

3.2.1 PWC with one excluding variable using the new method

Fig. 1 shows PWC between dependent variable y (or z) and predictor variable y_2 (or z_2) by excluding one variable. For the stationary case, there is one horizontal band (red color) representing an in-phase high PWC value at scales around 8 for all locations after eliminating the effect of y_4 (Fig. 1a). Note that the PWC values between y and y_2 after excluding the effect of y_4 are not exactly 1 as would be expected at all location-scale domains, because of the effect of smoothing along locations and scales. However, the PWC values at the center of the significance band, which corresponds to the predictor variable y_2 at exactly the scale of 8, are very close to 1 (0.996), and the mean PWC_{sig} values are very high (i.e., 0.96). The result is similar to the BWC between y and y_2. This is understandable because y_4 is orthogonal to y_2, and excluding the effect of y_4 does not affect the relationship between y and y_2 at all.

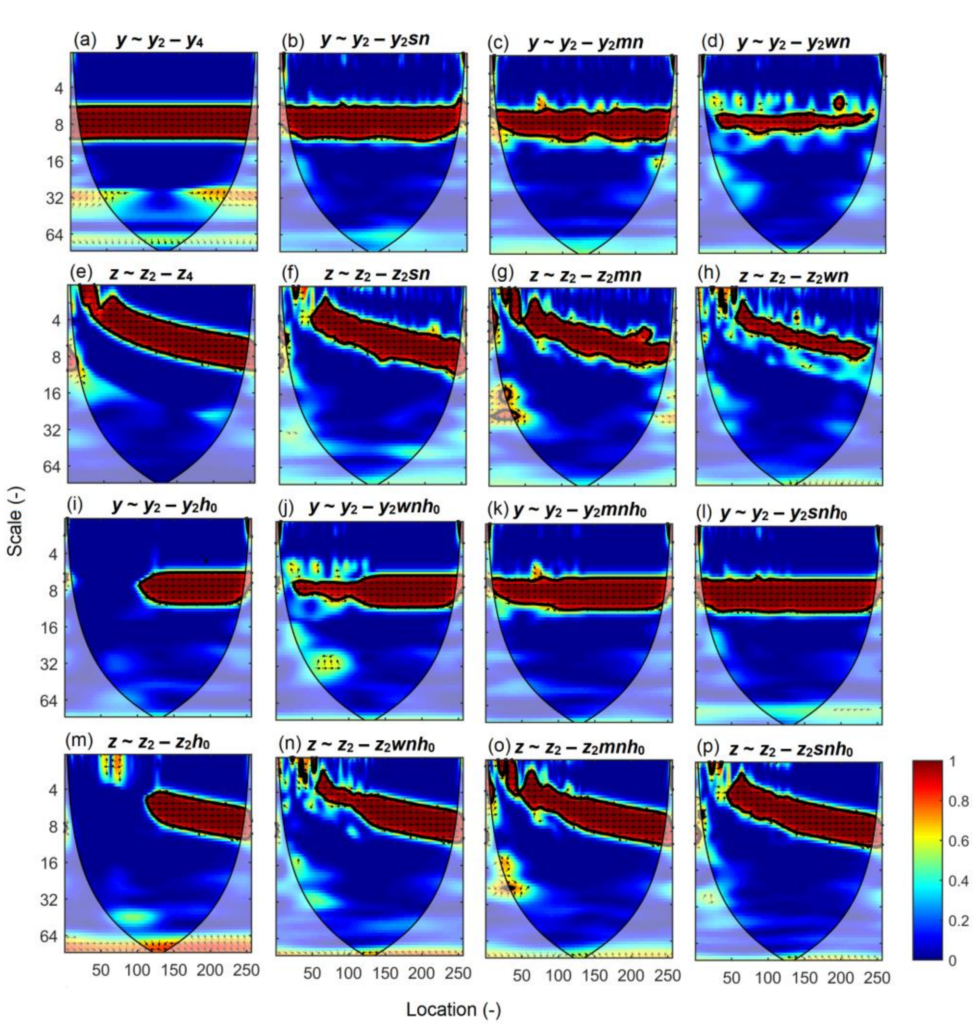

Figure 1.

Partial wavelet coherency (PWC) between response variable y (or z) and predictor variable

y_2 (or z_2) after excluding the effect of variables y_4 (or z_4), y_2sn (or z_2sn), y_2mn (or z_2mn), y_2wn (or z_2wn), y_2h_0 (or z_2h_0), y_2wnh_0 (or z_2wnh_0), y_2mnh_0 (or z_2mnh_0), and y_2snh_0 (or z_2snh_0) for the stationary (or non-stationary) case using the new method. Arrows represent the phase angles of the cross-wavelet power spectra between two variables after eliminating the effect of excluding variables. Arrows pointing to the right (left) indicate positive (negative) correlations. Thin and thick solid lines show the cones of influence and the 95% confidence levels, respectively. All variables were generated by following Yan and Gao (2007) and Hu and Si (2016) and are explained in Section 3.1 and shown in Fig. S2 of Sect. S3 in the Supplement**.**

Similar results were obtained by excluding either y_4 or the strongly noised series of y_2 (y_2sn). Compared with the case of excluding variable of y_4 (Fig. 1a), excluding the effect of y_2sn (Fig. 1b) results in slightly narrower band of significant PWC and slightly reduced mean PWC_{sig} (0.94 versus 0.96). When less noise is included in the excluding variables (i.e., y_2mn and y_2wn) (Fig. 1c-d), the significant PWC band becomes narrower. The PASC values are 86%, 77%, and 32% for excluding y_2sn, y_2mn and y_2wn, respectively, at scales of 6–10. Moreover, the mean PWC_{sig} decreases from 0.94 (y_2sn) to 0.93 (y_2mn) and 0.89 (y_2wn) when progressively more noise is added (Fig. 1b-d). For the non-stationary case, similar results are obtained (Fig. 1e-h). The only difference is that the scales with significant PWC values change with location, as is found for MWC (Hu and Si, 2016).

When the second half of the excluding variable series is replaced by 0, the PWC values in that half are close to 1, while those in the first half of data series are 0 at scales corresponding to the predictor variable (Fig. 1i and 1m). For the stationary case, after excluding the effect of y_2h_0, the PWC values are close to 1 (0.98) and 0 in the second and first half of the data series, respectively, at the dimensionless scale of 8 (Fig. 1i). Similar results are observed for the non-stationary case (Fig. 1m). This is anticipated because the removing series of 0s from a portion of the predictor variable series does not affect their correlations at these locations. If different magnitudes of noises are added to the first half of the excluding variables (y_2 or z_2), the significant PWC band in the first half becomes wider as the magnitude of noises increases, while the significant PWC band in the second half remains almost unchanged (Fig. 1j-l and Fig. 1n-p). In the stationary case, for example, the PASC values at scales of 6–10 are 40% (y_2wnh_0), 74% (y_2mnh_0), and 86% (y_2snh_0) in the first half, while those values vary from 86% to 90% in the second half (Fig. 1j-l). Meanwhile, the mean PWC_{sig} in the first half at scales of 6–10 increases from 0.91 to 0.94 in both the stationary (Fig. 1j-l) and non-stationary (Fig. 1n-p) cases as more noises are added to the excluding variable y_2 or z_2. This indicates that the new PWC method can also capture the abrupt changes (Fig. 1i and 1m) in the data series, and has the ability to deal with localized relationships.

3.2.2 PWC with two excluding variables using the new method

When both y_2 and y_4 (or z_2 and z_4) are considered in the predictor variables, there are two bands of wavelet coherence of 1 between y (or z) and y_2y_4 (or z_2z_4) (Hu and Si, 2016), which correspond to the scales of two predictor variables. However, after the effect of y_4 (or z_4) is removed, only one band with PWC of around 1 occurs at the scale of the predictor variable y_2 (or z_2) (Fig. 2a and 2f), which is identical to the PWC between y (or z) and y_2 (or z_2) after excluding the effect of variable y_4 (or z_4) (Fig. 1a and 1f). After both predictor variables y_2 and y_4 (or z_2 and z_4) are excluded (Fig. 2b and 2g), the PWC between y (or z) and y_2y_4 (or

z_2z_4) is 0 at all location-scale domains as we expect. When one of the excluding variables y_2 (or z_2) is added with noises, the relationship between response variable y (or z) and predictor variable y_2y_4 (or z_2z_4) becomes significant at scales of the excluding variable y_2 (or z_2) (Fig. 2c and 2h). Similar to the case of one excluding variable (Fig. 1), less noise in the excluding variable of y_2 (or z_2) results in a narrower significant PWC band, and reduced mean PWC_{sig} values (from 0.96 (y_2sn) to 0.90 (y_2wn) in the stationary case (Fig. 2c-e) and from 0.95 (z_2sn) to 0.92 (z_2wn) in the non-stationary case) (Fig. 2h-j).

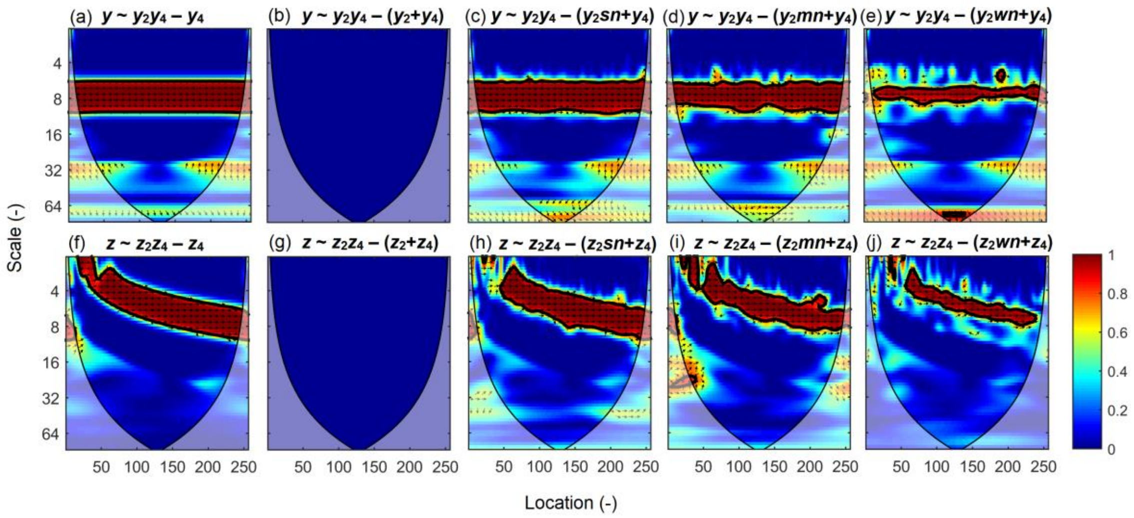

Figure 2.

Partial wavelet coherency (PWC) between response variable y (or z) and predictor variable y_2y_4 (or z_2z_4) after excluding the effect of variables y_4 (or z_4), y_2+y_4 (or z_2+z_4), $y_2$sn+y_4 (or z_2sn+z_4), y_2mn+y_4 (or z_2mn+z_4), and y_2wn+y_4 (or z_2wn+z_4) for the stationary (or non-stationary) case using the new method. All variables were generated by following Yan and Gao (2007) and Hu and Si (2016) and are explained in Section 3.1 and shown in Fig. S2 of Sect. S3 in the Supplement.

4. Method application with real dataset

4.1 Description of free water evaporation dataset

The free water evaporation dataset was used to test the MWC (Hu and Si, 2016). In brief, this dataset includes monthly free water evaporation (E), mean temperature (T), relative humidity (RH), sun hours (SH), and wind speed (WS) between January 1979 and December 2013 at Changwu site in Shaanxi province provided by the China Meteorological Administration. During this period, the average daily temperature was 9.4 °C, the average annual rainfall was 571 mm and annual ET_p was 883 mm. Being located in the transition between semi-arid and subhumid climates, agricultural production at the Changwu site is constrained by water availability. Results of wavelet power spectrum of E and BWC between every two variables are shown in Fig. S3 and Fig. S4 (Sect. S3 in the Supplement), respectively.

4.2 PWC with free water evaporation dataset

The PWC analysis indicates that the correlations between E and T after excluding the effect of each of other three variables (RH, SH, and WS) were almost the same as those indicated by the BWC (Fig. 3a-c and Fig. S4 of Sect. S3 in the Supplement). For example, E and T, after excluding the effect of RH, were positively correlated at the medium scales (8–32 months). The PASC was 61% and mean PWC_{sig} value was 0.94, which was identical to the case of BWC between E and T. No significant correlations at scales around 64 months between E and T from 1979 to 1992 were found after eliminating the influence of RH (Fig.

3a-c). This implies that the influence of mean temperature on E at these scales and years may be associated with the negative influence of RH on both E and T (Fig. S4 of Sect. S3 in the Supplement).

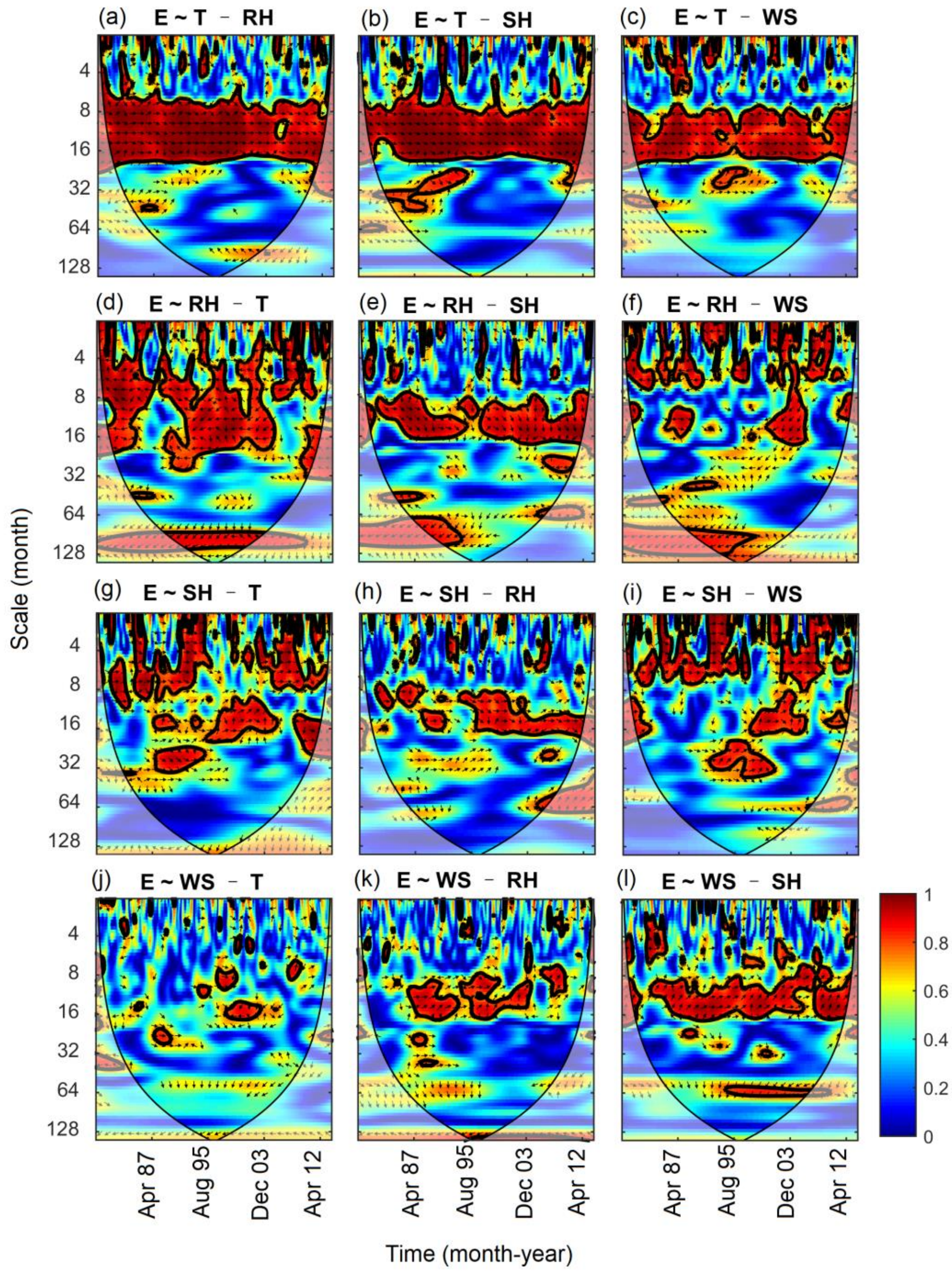

Figure 3.

Partial wavelet coherency (PWC) between evaporation (E) and each meteorological factor

(T, mean temperature; RH, relative humidity; SH, sun hours; WS, wind speed) after excluding the effect of each of other three meteorological factors.

The PWC between E and RH depended on the excluding variable and scale (Fig. 3d-f). The mean PWC and PASC between E and RH after excluding T were 0.60 and 34%, respectively, which are comparable with the mean BWC (0.62) and PASC (40%) between E and RH. The corresponding values after excluding SH and WS were 0.50 and 0.53 (PWC), 22% and 21% (PASC), respectively. In addition, compared with the BWC between E and RH (Fig. S4 of Sect. S3 in the Supplement), correlations between E and RH were weak at small scales (<8 months) and medium scales (8–32 months) after eliminating the influence of SH and WS (Fig. 3e-f), respectively. Therefore, excluding the variable of T had less influence on the coherence between E and RH compared with excluding the variables of SH and WS. This is mainly because RH and T are correlated with E at different scales (Fig. S4 of Sect. S3 in the Supplement), i.e., mean temperature affected E mainly at medium scales, while RH affected E across all scales. However, the domain where SH and WS were correlated with E was a subset of that where RH and E were correlated (Fig. S4 of Sect. S3 in the Supplement).

The relationships between E and SH after excluding the other three factors were less consistent (Fig. 3g-h). The areas with significant corrections were scattered over the whole location-scale domain but differed with excluding factors. The PASC varied from 12% (excluding RH) to 20% (excluding T and WS), which is much lower than the PASC (28%) in the case of BWC. The significant relationships between E and WS were only limited to very small areas except for the case of SH being excluded, where E and WS were positively correlated at scales of 8–16 months most of the time (Fig. 3j-l).

In general, the PASC decreased after excluding the effects of more factors (data not shown). The correlations between E and each variable after eliminating the effects of all other variables are shown in Fig. 4. The correlations between E and T were still significant at the medium scales (8–32 months) (Fig. 4a), where PASC value was 52% with mean PWC_{sig} of 0.92. The E was still correlated with RH at large scales (>32 months) (Fig. 4b), where PASC value was 35% with mean PWC_{sig} of 0.96. Interestingly, the domain with significant correlation between E and SH and WS was very limited (Fig. 4c-d). This indicates that the influences of SH and WS on E have already been covered by RH and T. This is in agreement with the MWC results that RH and T were the best to explain E variations at all scales (Hu and Si, 2016). Although the RH had the greatest mean wavelet coherence and PASC at the entire location-scale domains, the PWC analysis seems to support that mean temperature was the most dominating factor for free water evaporation at the 1-year cycle (8–16 months), which is the dominant scale of E variation (Fig. S3 of Sect. S3 in the Supplement).

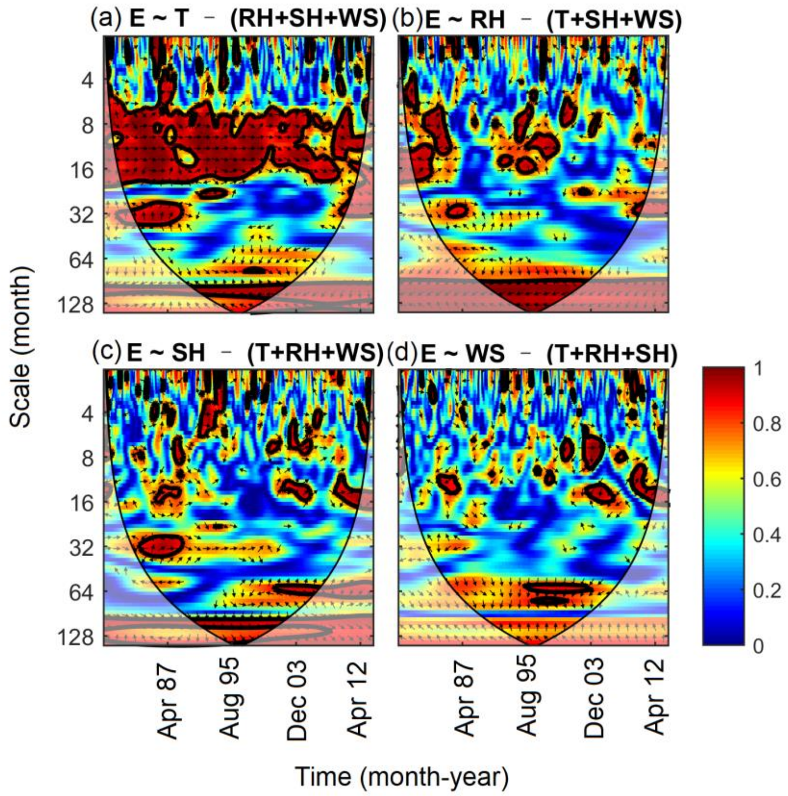

Figure 4.

Partial wavelet coherency (PWC) between evaporation (E) and each meteorological factor (T, mean temperature; RH, relative humidity; SH, sun hours; WS, wind speed) after excluding the effects of all other three factors.

5. Discussion on the advantages and weaknesses of the new method

5.1 Advantages

We extend the partial coherence method from the frequency (scale) domain (Koopmans, 1995) to the time-frequency (location-scale) domain. The new method is an extension of previous work on PWC and MWC (Mihanović et al., 2009; Hu and Si, 2016). The method test and application have verified that it has the advantage of dealing with more than one excluding variable and providing the phase information associated with the PWC. In the case of one excluding variable, Mihanović et al. (2009) has suggested to calculate PWC by using an equation analogous to the traditional partial correlation squared (Eq. 14), which can be derived from our Eq. (9). However, their equation was, unfortunately, widely used by replacing the complex coherence in Eq. (14) with real coherence as expressed in Eq. (15).

The differences between the new method (Eq.14) and the classical method (Eq. 15) are compared using both the artificial and real datasets. Except for the phase information, the two methods generally produce comparable coherence for the artificial dataset for the case of one excluding variable (Fig. S5 of Sect. S3 in the Supplement). However, the new PWC method produces consistently and slightly higher coherence than the classical method. For example, their mean PWCs between y and y_2 at the scale of 8 after excluding the effect of y_4 are 1.00 and 0.97, respectively. This indicates that the new method produces coherence between y and y_2 at the scale (8) of y_2 closer to 1 as we expect. While the classical method produces similar PWC between E and other meteorological factors in most cases especially for the coherence between E and T after excluding the effects of others (Fig. S6 of Sect. S3 in the Supplement), large differences between these two methods can also be observed. For example, while the new method recognizes the strong coherence between E and RH after excluding the effect of T at scales of around 1 year (Fig. 3d), this coherence was negligible by the classical method (Fig. 5a). Mean PWC values by the new method were consistently higher than the classical method, and the differences ranged from 0.4 to 0.6 around the scale of 1 year (Fig. 5b). Considering the real coherence (Eq.15) rather than complex coherence (Eq.14) between every two variables in the numerators can potentially result in large underestimation of the partial wavelet coherence. Therefore, the ability of the new method to produce more accurate results than the classical method is one of its advantages.

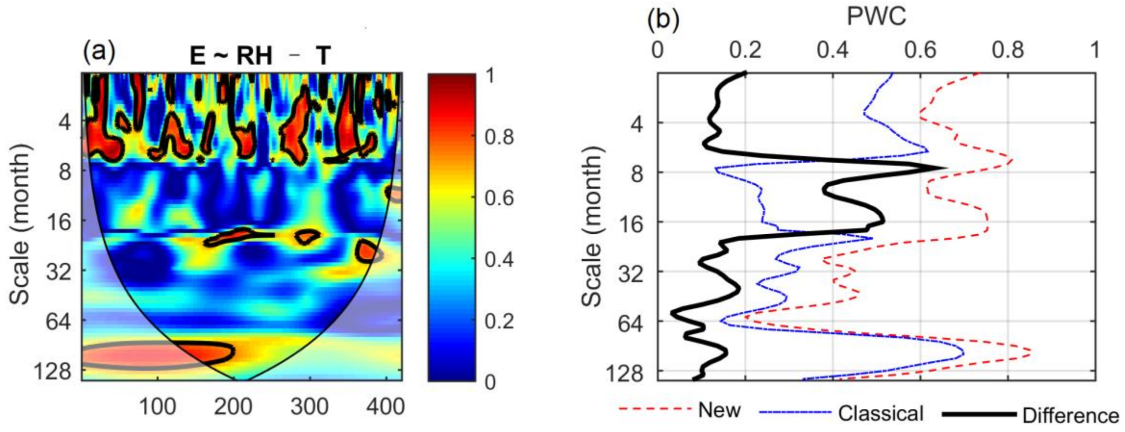

Figure 5.

Partial wavelet coherency (PWC) between evaporation (E) and relative humidity (RH) after excluding the effect of mean temperature (T) using the classical method (Eq. 15) (a) and differences in PWC between the new method (Eq.14) and classical method as a function of scale (b).

Compared with the Mihanović et al. (2009) method, the additional phase information from the new PWC is another advantage of this new method. This is because phase information is directly related to the type of correlation, i.e., in-phase and out-of-phase indicating positive and negative correlation, respectively. Different types of correlations were usually found at different locations and scales (Hu et al., 2017). The phase information helps understand the differences in associated mechanisms or processes at different locations and scales. In addition, the phase information will allow us to detect the changes in not only the degree of correlation (i.e., coherence) but also the type of correlation after excluding the effect of other variables. For example, E and RH were positively correlated at the 1-year cycle (8–16 months) from year 1979 to 1995. This is because higher evaporation usually occurs in summer when high T coincides with high RH as influenced by the monsoon climate in the study area (Fig. S4 of Sect. S3 in the Supplement). Interestingly, after excluding the effect of T, E was negatively correlated with RH at the scale of 1-year as we expect (Fig. 3d).

Moreover, our new PWC method applies to cases with more than one excluding variable, which is a knowledge gap. When multiple variables are correlated with both the predictor and response variables, the correlations between predictor and response variables may be misleading if the effects of all these multiple variable were not removed. For example, at the dominant scale (i.e., 1-year) of E variation, the effects of RH on E existed after excluding the effects of T or SH. However, their contrasting correlations (Fig. 3d-e) resulted in negligible effects of RH on E at this scale after the effects of all other variables were excluded (Fig. 4b). In this case, the dominant role of mean temperature in driving free water evaporation was proved at the 1-year cycle (Fig. 4a). This also further verifies the suitability of the Hargreaves model (only air temperature and incident solar radiation required) (Hargreaves, 1989) for estimating potential evapotranspiration on the Chinese Loess Plateau (Li, 2012).

5.2 Weaknesses

Similar to the Mihanović et al. (2009) method, the new method has the risk to produce spurious high correlations after excluding the effect from other variables. Take the artificial dataset for example, at a scale of 32, PWC values between y and y_2 after excluding y_4 are not significant, but relatively high, partly because of small octaves per scale (octave refers to the scaled distance between two scales with one scale being twice or half of the other, default of 1/12). This spurious unexpected high PWC is caused by low values in both the numerator (partly associated with the low coherence between response y and predictor variables y_2 at scale of 32) and denominator (partly associated with the high coherence between response y and excluding variable y_4 at a scale of 32) in Eq. (9). The same problem also exists in the classical method (Fig. S5 of Sect. S3 in the Supplement). So, caution should be taken to interpret those results. However, it seems that the domain with spurious correlation calculated by the new method is very limited and it is located mainly outside of the cones of influence. Moreover, the unexpected results can be easily ruled out with knowledge of BWC between response and predictor variables. It is expected that the correlation between two variables should not increase after excluding one or more variables. Therefore, BWC analysis is suggested for better interpretation of the PWC results.

Similar to BWC and MWC, the confidence level of PWC calculated from the Monte Carlo simulation is based on a single hypothesis testing. But in reality, the confidence level of PWC values at all locations and scales needs to be tested simultaneously. Therefore, the significance test has the multiple-testing problem (Schaefli et al., 2007; Schulte et al., 2015). The new method may benefit from a better statistical significance testing method. Options for multiple-testing can be the Bonferroni adjusted p test (Westfall and Young, 1993) or false discovery rate (Abramovich and Benjamini, 1996; Shen et al., 2002) which is less stringent than the former.

6. Conclusions

Partial wavelet coherency (PWC) is developed in this study to investigate scale-specific and localized bivariate relationships after excluding the effect of one or more variables in geosciences. Method tests using stationary and non-stationary artificial datasets verified the known scale- and localized bivariate relationships after eliminating the effects of other variables. Compared with the previous PWC method, the new PWC method has the advantage of dealing with more than one excluding variable and providing the phase information (i.e., correlation type) associated with the PWC. In the case of one excluding variable, this new method produces more accurate coherence than the previous PWC method because the former considers complex coherence between every two variables, while the latter only considers the real coherence. Application of the new method to one temporal dataset (free water evaporation) has indicated the robustness of the new method in identifying the bivariate relationships and further convinced the MWC method in identifying the best combinations for explaining variations. The new method provides a much needed data-driven tool for unraveling underlying mechanisms in both temporal and spatial series. Thus, combining with wavelet transform, BWC, and MWC, the new PWC method can be used to detect various processes in geosciences, such as stream flow, droughts, greenhouse gas emissions (e.g., N_2O, CO_2, and CH_4), atmospheric circulation, and oceanic processes (e.g., EI Niño-Southern Oscillation).

Code/Data availability

The Matlab codes for calculating PWC, along with the updated MWC codes, are freely accessible (https://figshare.com/s/bc97956f43fe5734c784). The codes are developed based on those provided by Aslak Grinsted (http://www.glaciology.net/wavelet-coherence). The meteorological data sets can be obtained from the China Meteorological Administration.

Author contributions

WH wrote the paper, did the Matlab code development, and analyzed the data. Both authors conceived the study, interpreted the results, and revised the paper.

Competing interests

The authors declare that they have no conflict of interest.

Acknowledgements

The preparation of this manuscript was supported by The New Zealand Institute for Plant and Food Research Limited under the Sustainable Agro-ecosystems programme.

References

Abramovich, F. and Benjamini, Y.: Adaptive thresholding of wavelet coefficients, Computational Statistics & Data Analysis, 22, 351-361, 1996.

Aloui, C., Hkiri, B., Hammoudeh, S., and Shahbaz, M.: A multiple and partial wavelet analysis of the oil price, inflation, exchange rate, and economic growth nexus in Saudi Arabia, Emerging Markets Finance and Trade, 54, 935-956, 2018.

Altarturi, B. H., Alshammari, A. A., Saiti, B., and Erol, T.: A three-way analysis of the relationship between the USD value and the prices of oil and gold: A wavelet analysis, AIMS Energy, 6, 487, 2018a.

Altarturi, B. H. M., Alshammari, A. A., Saiti, B., and Erol, T.: A three-way analysis of the relationship between the USD value and the prices of oil and gold: A wavelet analysis, Aims Energy, 6, 487-504, 2018b.

Biswas, A. and Si, B. C.: Identifying scale specific controls of soil water storage in a hummocky landscape using wavelet coherency, Geoderma, 165, 50-59, 2011.

Centeno, L. N., Hu, W., Timm, L. C., She, D. L., Ferreira, A. D., Barros, W. S., Beskow, S., and Caldeira, T. L.: Dominant Control of Macroporosity on Saturated Soil Hydraulic Conductivity at Multiple Scales and Locations Revealed by Wavelet Analyses, Journal of Soil Science and Plant Nutrition, 20, 2020.

Das, N. N. and Mohanty, B. P.: Temporal dynamics of PSR-based soil moisture across spatial scales in an agricultural landscape during SMEX02: A wavelet approach, Remote Sensing of Environment, 112, 522-534, 2008.

Graf, A., Bogena, H. R., Drüe, C., Hardelauf, H., Pütz, T., Heinemann, G., and Vereecken, H.: Spatiotemporal relations between water budget components and soil water content in a forested tributary catchment, Water Resour Res, 50, 4837-4857, 2014.

Grinsted, A., Moore, J. C., and Jevrejeva, S.: Application of the cross wavelet transform and wavelet coherence to geophysical time series, Nonlinear Processes in Geophysics, 11, 561-566, 2004.

Gu, X. F., Sun, H. G., Tick, G. R., Lu, Y. H., Zhang, Y. K., Zhang, Y., and Schilling, K.: Identification and Scaling Behavior Assessment of the Dominant Hydrological Factors of Nitrate Concentrations in Streamflow, J Hydrol Eng, 25, 06020002, 2020.

Hargreaves, G. H.: Accuracy of estimated reference crop evapotranspiration, Journal of irrigation and drainage engineering, 115, 1000-1007, 1989.

Hu, W. and Si, B. C.: Technical note: Multiple wavelet coherence for untangling scale-specific and localized multivariate relationships in geosciences, Hydrol Earth Syst Sc, 20, 3183-3191, 2016.

Hu, W., Si, B. C., Biswas, A., and Chau, H. W.: Temporally stable patterns but seasonal dependent controls of soil water content: Evidence from wavelet analyses, Hydrol Process, 31, 3697-3707, 2017.

Jia, X., Zha, T., Gong, J., Zhang, Y., Wu, B., Qin, S., and Peltola, H.: Multi-scale dynamics and environmental controls on net ecosystem CO_2 exchange over a temperate semiarid shrubland, Agricultural and Forest Meteorology, 259, 250-259, 2018.

Kenney, J. F. and Keeping, E. S.: Mayhematics of Statistics, D. van Nostrand, 1939.

Koopmans, L. H.: The spectral analysis of time series, Elsevier, 1995.

Lakshmi, V., Piechota, T., Narayan, U., and Tang, C.: Soil moisture as an indicator of weather extremes, Geophysical research letters, 31, L11401, 2004.

Li, H., Dai, S., Ouyang, Z., Xie, X., Guo, H., Gu, C., Xiao, X., Ge, Z., Peng, C., and Zhao, B.: Multi-scale temporal variation of methane flux and its controls in a subtropical tidal salt marsh in eastern China, Biogeochemistry, 137, 163-179, 2018.

Li, Z.: Applicability of simple estimating method for reference crop evapotranspiration in Loess Plateau, Transactions of the Chinese Society of Agricultural Engineering, 28, 106-111, 2012.

Mares, I., Mares, C., Dobrica, V., and Demetrescu, C.: Comparative study of statistical methods to identify a predictor for discharge at Orsova in the Lower Danube Basin, Hydrological Sciences Journal, 65, 371-386, 2020.

Mihanović, H., Orlić, M., and Pasarić, Z.: Diurnal thermocline oscillations driven by tidal flow around an island in the Middle Adriatic, Journal of Marine Systems, 78, S157-S168, 2009.

Mutascu, M. and Sokic, A.: Trade openness-CO_2 emissions nexus: a wavelet evidence from EU, Environmental Modeling & Assessment, 25, 1-18, 2020.

Nalley, D., Adamowski, J., Biswas, A., Gharabaghi, B., and Hu, W.: A multiscale and multivariate analysis of precipitation and streamflow variability in relation to ENSO, NAO and PDO, J Hydrol, 574, 288-307, 2019.

Ng, E. K. and Chan, J. C.: Geophysical applications of partial wavelet coherence and multiple wavelet coherence, Journal of Atmospheric and Oceanic Technology, 29, 1845-1853, 2012a.

Ng, E. K. and Chan, J. C.: Interannual variations of tropical cyclone activity over the north Indian Ocean, International Journal of Climatology, 32, 819-830, 2012b.

Polansky, L., Wittemyer, G., Cross, P. C., Tambling, C. J., and Getz, W. M.: From moonlight to movement and synchronized randomness: Fourier and wavelet analyses of animal location time series data, Ecology, 91, 1506-1518, 2010.

Rathinasamy, M., Agarwal, A., Parmar, V., Khosa, R., and Bairwa, A.: Partial wavelet coherence analysis for understanding the standalone relationship between Indian Precipitation and Teleconnection patterns, arXiv preprint arXiv:1702.06568, 2017. 2017.

Schaefli, B., Maraun, D., and Holschneider, M.: What drives high flow events in the Swiss

Alps? Recent developments in wavelet spectral analysis and their application to hydrology, Adv Water Resour, 30, 2511-2525, 2007.

Schulte, J., Duffy, C., and Najjar, R.: Geometric and topological approaches to significance testing in wavelet analysis, Nonlinear Processes in Geophysics, 22, 2015.

Sen, A., Chaudhury, P., and Dutta, K.: On the co-movement of crude, gold prices and stock index in Indian market, arXiv preprint arXiv:1904.05317, 2019. 2019.

Shen, X., Huang, H.-C., and Cressie, N.: Nonparametric hypothesis testing for a spatial signal, Journal of the American Statistical Association, 97, 1122-1140, 2002.

Si, B. C.: Spatial scaling analyses of soil physical properties: A review of spectral and wavelet methods, Vadose Zone Journal, 7, 547-562, 2008.

Si, B. C. and Farrell, R. E.: Scale-dependent relationship between wheat yield and topographic indices: A wavelet approach, Soil Sci Soc Am J, 68, 577-587, 2004.

Si, B. C. and Zeleke, T. B.: Wavelet coherency analysis to relate saturated hydraulic properties to soil physical properties, Water Resour Res, 41, W11424, 2005.

Song, X. M., Zhang, C. H., Zhang, J. Y., Zou, X. J., Mo, Y. C., and Tian, Y. M.: Potential linkages of precipitation extremes in Beijing-Tianjin-Hebei region, China, with large-scale climate patterns using wavelet-based approaches, Theoretical and Applied Climatology, 141, 1251-1269, 2020.

Su, L., Miao, C., Duan, Q., Lei, X., and Li, H.: Multiple‐wavelet coherence of world's large rivers with meteorological factors and ocean signals, Journal of Geophysical Research: Atmospheres, 124, 4932-4954, 2019.

Tan, X., Gan, T. Y., and Shao, D.: Wavelet analysis of precipitation extremes over Canadian ecoregions and teleconnections to large‐scale climate anomalies, Journal of Geophysical Research: Atmospheres, 121, 14469-14486, 2016.

Torrence, C. and Compo, G. P.: A practical guide to wavelet analysis, Bulletin of the American Meteorological society, 79, 61-78, 1998.

Wendroth, O., Alomran, A. M., Kirda, C., Reichardt, K., and Nielsen, D. R.: State-Space Approach to Spatial Variability of Crop Yield, Soil Sci Soc Am J, 56, 801-807, 1992.

Westfall, P. H. and Young, S. S.: Resampling-based multiple testing: Examples and methods for p-value adjustment, John Wiley & Sons, 1993.

Wu, K., Zhu, J., Xu, M., and Yang, L.: Can crude oil drive the co-movement in the international stock market? Evidence from partial wavelet coherence analysis, The North American Journal of Economics and Finance, 2020. 101194, 2020.

Yan, R. and Gao, R. X.: A tour of the tour of the Hilbert-Huang transform: an empirical tool for signal analysis, IEEE Instrumentation & Measurement Magazine, 10, 40-45, 2007.

Zhao, R., Biswas, A., Zhou, Y., Zhou, Y., Shi, Z., and Li, H.: Identifying localized and scale-specific multivariate controls of soil organic matter variations using multiple wavelet coherence, Sci Total Environ, 643, 548-558, 2018.